

Status of the S_8 Tension: A 2026 Review of Probe Discrepancies

Ioannis Pantos and Leandros Perivolaropoulos

Department of Physics, University of Ioannina
Ioannina 45110, Greece

February 13, 2026

Abstract

The parameter $S_8 \equiv \sigma_8(\Omega_m/0.3)^{0.5}$ quantifies the amplitude of matter density fluctuations. A persistent discrepancy exists between early-universe CMB observations and late-universe probes. This review assesses the “ S_8 tension” against a new 2026 baseline: a unified “Combined CMB” framework incorporating Planck, ACT DR6, and SPT-3G. This combined analysis yields $S_8 = 0.836^{+0.012}_{-0.013}$, providing a higher central value and reduced uncertainties compared to Planck alone. Compiling measurements from 2019–2026, we reveal a striking bifurcation: DES Year 6 results exhibit a statistically significant tension of 2.4σ – 2.7σ (Abbott *et al.*, 2026), whereas KiDS Legacy results demonstrate statistical consistency at $< 1\sigma$ (Wright *et al.*, 2025). We examine systematic origins of this dichotomy, including photometric redshift calibration, intrinsic alignment modeling, and shear measurement pipelines. We further contextualize these findings with cluster counts (where eROSITA favors high values while SPT favors low), galaxy-galaxy lensing, and redshift-space distortions. The heterogeneous landscape suggests survey-specific systematic effects contribute substantially to observed discrepancies, though new physics beyond Λ CDM cannot be excluded.

Contents

1	Introduction	3
1.1	The Emergence of Precision Cosmology	3
1.2	The S_8 Parameter: Definition and Significance	3
1.3	Historical Context: The Evolution of the S_8 Tension	4
1.4	The 2026 Paradigm Shift: Combined CMB as the New Baseline	4
2	Methodology: Quantifying Cosmological Tensions	4
2.1	Statistical Framework for Tension Assessment	4
2.2	Treatment of Asymmetric Uncertainties	5
2.3	Correlation Between Measurements	5
3	The Combined CMB Baseline: Technical Details	5
3.1	Component Datasets	5
3.1.1	Planck 2018	6
3.1.2	ACT Data Release 6	6
3.1.3	SPT-3G	6
3.2	Combination Methodology	6
4	Late-Universe Probes: Physical Principles and Systematic Uncertainties	7
4.1	Weak Gravitational Lensing	7
4.1.1	Systematic Uncertainties in Cosmic Shear	7
4.2	Galaxy Clustering and the 3×2 pt Framework	8
4.3	Galaxy Cluster Counts	9
4.4	Redshift-Space Distortions	9

5 Compilation of S_8 Measurements (2019–2026)	10
5.1 Visual Summary	10
5.2 Detailed Tabulation	11
6 Analysis of Key Results	13
6.1 The Dark Energy Survey Year 6 Analysis	13
6.1.1 Methodological Advances	13
6.1.2 Results and Tension Assessment	13
6.1.3 Extended Cosmological Models	13
6.2 Evolution from KiDS-1000 to Legacy	14
6.2.1 Implications for the Tension Landscape	14
6.3 The eROSITA Cluster Count Anomaly	14
6.3.1 Physical Interpretation	14
6.3.2 Comparison with Other Cluster Samples	14
6.4 Spectroscopic Probes: DESI and RSD Measurements	14
6.5 Galaxy-Galaxy Lensing and Alternative Probes	15
7 Systematic Effects: A Critical Assessment	15
7.1 Photometric Redshift Calibration	15
7.2 Shear Measurement Systematics	15
7.3 Intrinsic Alignments	16
7.4 Baryon Feedback and Nonlinear Modeling	16
8 Theoretical Interpretations	16
8.1 Consistency within Λ CDM	16
8.2 Modified Gravity	16
8.3 Interacting Dark Sector	17
8.4 Evolving Dark Energy	17
9 Discussion and Future Outlook	17
9.1 Summary of the Current Tension Landscape	17
9.2 Paths to Resolution	18
9.3 Concluding Remarks	18

1 Introduction

1.1 The Emergence of Precision Cosmology

The past three decades have transformed cosmology from a largely qualitative discipline into a precision science. The establishment of the Λ CDM concordance model—characterized by a cosmological constant Λ , cold dark matter, baryonic matter, and a nearly scale-invariant spectrum of primordial perturbations—represents one of the most significant achievements in modern physics. This model successfully describes observations spanning fourteen orders of magnitude in scale, from the acoustic peaks in the CMB power spectrum to the distribution of galaxies in the cosmic web.

The parameters of the Λ CDM model have been constrained with remarkable precision through a diverse array of cosmological probes. Primary among these are observations of the CMB, which encode information about the universe at the epoch of recombination approximately 380,000 years after the Big Bang. The *Planck* satellite, operational from 2009 to 2013, provided the definitive space-based measurement of CMB temperature and polarization anisotropies (Planck Collaboration *et al.*, 2020), achieving cosmic variance-limited measurements over a substantial fraction of the sky and across a wide range of angular scales.

The concordance between independent cosmological probes has been a cornerstone of modern cosmology’s success. However, as measurement precision has improved, subtle but persistent discrepancies have emerged. The most prominent of these—the Hubble tension between early- and late-universe determinations of H_0 —has garnered substantial attention. Less widely discussed but equally intriguing is the tension in measurements of the amplitude of matter clustering, parameterized by S_8 .

1.2 The S_8 Parameter: Definition and Significance

Among the parameters characterizing the Λ CDM model, the amplitude of matter density fluctuations holds particular importance for understanding structure formation. This amplitude is conventionally parameterized by σ_8 , defined as the root-mean-square of the linear matter density field when smoothed with a top-hat filter of radius $8 h^{-1}$ Mpc:

$$\sigma_8^2 = \int_0^\infty \frac{k^2 P(k)}{2\pi^2} |W(kR)|^2 dk, \quad (1)$$

where $P(k)$ is the linear matter power spectrum, $W(kR)$ is the Fourier transform of the top-hat window function, and $R = 8 h^{-1}$ Mpc. The choice of $8 h^{-1}$ Mpc is historical, corresponding roughly to the scale at which the variance of galaxy counts in spheres equals unity.

Late-universe probes of large-scale structure, particularly weak gravitational lensing surveys, exhibit a characteristic degeneracy between σ_8 and the matter density parameter Ω_m . This degeneracy arises because cosmic shear measurements are sensitive to the integrated matter power spectrum along the line of sight, weighted by geometric lensing kernels. The resulting constraints trace out elongated contours in the σ_8 – Ω_m plane, approximately following curves of constant $S_8 \equiv \sigma_8(\Omega_m/0.3)^\alpha$, where the exponent α depends on the specific observable and redshift distribution but typically falls in the range 0.4–0.6. The conventional choice $\alpha = 0.5$ has been adopted as a standard, yielding:

$$S_8 \equiv \sigma_8 \sqrt{\frac{\Omega_m}{0.3}}. \quad (2)$$

This combination is particularly well-constrained by weak lensing measurements and serves as the primary diagnostic for comparing early- and late-universe determinations of the clustering amplitude. As emphasized by Amon and Efstathiou (2022), the interpretation of S_8 constraints requires careful attention to the scales being probed and potential systematic effects that may differ between linear and nonlinear regimes.

1.3 Historical Context: The Evolution of the S_8 Tension

The S_8 tension first emerged as a statistically significant discrepancy following the *Planck* 2015 data release, which reported $S_8 = 0.851 \pm 0.024$ under the assumption of a flat Λ CDM cosmology. Contemporary weak lensing analyses from the Canada-France-Hawaii Telescope Lensing Survey (CFHTLenS) and early results from KiDS consistently favored lower values, typically in the range $S_8 \approx 0.75\text{--}0.78$. The statistical significance of this discrepancy ranged from $2\sigma\text{--}3\sigma$ depending on the specific datasets and analysis choices employed.

The *Planck* 2018 final data release refined the CMB-based constraint to $S_8 = 0.832 \pm 0.013$ (Planck Collaboration *et al.*, 2020), a modest downward revision that nonetheless maintained tension with the majority of weak lensing measurements. Throughout the period 2018–2024, multiple independent weak lensing analyses—including KiDS-1000 (Asgari *et al.*, 2021), DES Year 3 (Abbott *et al.*, 2022) $\sim 2.6\sigma$ relative to *Planck*, and HSC Year 1 (Hikage *et al.*, 2019) $\sim 1.6\sigma$ —reported S_8 values systematically below the *Planck* prediction, with typical discrepancies of $\sim 1.6\sigma$ to $\sim 2.7\sigma$.

The persistence of this tension across multiple independent surveys lent credibility to the hypothesis that it might reflect genuine new physics rather than systematic errors. Proposed explanations have included modifications to gravity (Boiza *et al.*, 2025; Souza *et al.*, 2025; Terasawa *et al.*, 2025; Hu and Sawicki, 2007), decaying dark matter (Tanimura *et al.*, 2023), interacting dark energy (Sabogal *et al.*, 2024), and various extensions to the neutrino sector. However, as we shall discuss, the heterogeneous nature of the current tension landscape complicates such interpretations.

1.4 The 2026 Paradigm Shift: Combined CMB as the New Baseline

The cosmological landscape underwent a significant transformation in early 2026 with the maturation of ground-based CMB experiments to a precision level rivaling and complementing *Planck*. The Atacama Cosmology Telescope (ACT) Data Release 6 (Louis *et al.*, 2025) and the South Pole Telescope 3rd Generation (SPT-3G) (Camphuis *et al.*, 2025) now provide high-resolution measurements of the CMB damping tail at multipoles $\ell > 2000$, where *Planck*’s angular resolution becomes limiting. These ground-based experiments also offer independent measurements of CMB lensing (Madhavacheril *et al.*, 2024), providing crucial cross-checks on systematic uncertainties.

The combination of *Planck* 2018, ACT DR6, and SPT-3G data—referred to throughout this review as the “Combined CMB” dataset—yields a constraint of $S_8 = 0.836^{+0.012}_{-0.013}$ (Abbott *et al.*, 2026). This represents several important developments relative to the *Planck*-only baseline:

1. The central value has shifted upward by approximately 0.004, or roughly 0.3σ in the *Planck* error budget.
2. The uncertainties remain comparable to the *Planck*-only case, with a slight reduction in the upper uncertainty from $+0.013$ to $+0.012$.
3. The combination of independent experiments with different systematic error profiles enhances confidence in the robustness of the result.

This review adopts the Combined CMB baseline as the primary reference against which late-universe measurements are compared. Where relevant, we also discuss tensions relative to the *Planck* 2018 baseline for historical context and comparison with earlier literature.

2 Methodology: Quantifying Cosmological Tensions

2.1 Statistical Framework for Tension Assessment

Before presenting the compilation of S_8 measurements, it is essential to establish the statistical framework employed for quantifying tensions between datasets. Several approaches exist in the

literature, each with distinct advantages and limitations.

The simplest and most commonly employed metric is the difference in mean values normalized by the combined uncertainty:

$$n_\sigma = \frac{|S_8^{(A)} - S_8^{(B)}|}{\sqrt{\sigma_A^2 + \sigma_B^2}}, \quad (3)$$

where $S_8^{(A)}$ and $S_8^{(B)}$ are the central values from datasets A and B, and σ_A and σ_B are the corresponding uncertainties. This metric assumes Gaussian posteriors and statistical independence between the datasets.

More sophisticated tension metrics have been developed to overcome limitations of the simple n_σ approach. Handley and Lemos (2019) introduced the Suspiciousness statistic, a prior-insensitive Bayesian method that accounts for the full multi-dimensional parameter space. Tröster *et al.* (2020) employed both the Bayesian evidence ratio and Suspiciousness statistic to quantify the S_8 discrepancy, finding a $2.1 \pm 0.3\sigma$ tension between combined BOSS galaxy clustering and KV450 weak lensing data and Planck CMB constraints—broadly consistent with simpler metrics when posteriors are approximately Gaussian.

In cases where posteriors are significantly non-Gaussian or exhibit complex degeneracies, these methods may yield tension assessments that differ from the simple n_σ metric. Throughout this review, we report tensions using the n_σ metric for consistency and ease of comparison, while noting cases where more detailed statistical analyses have been performed and yield different conclusions.

2.2 Treatment of Asymmetric Uncertainties

Many S_8 measurements report asymmetric uncertainties, reflecting non-Gaussian posterior distributions. For such cases, we adopt the convention of using the uncertainty in the direction of the discrepancy when computing n_σ . Specifically, when comparing a measurement $S_8 = x_{-\sigma_2}^{+\sigma_1}$ against the Combined CMB baseline ($S_8 = 0.836_{-0.013}^{+0.012}$), we use σ_2 and the baseline lower uncertainty if $x < 0.836$, and σ_1 and the baseline upper uncertainty if $x > 0.836$.

2.3 Correlation Between Measurements

A significant complication in assessing the global significance of the S_8 tension arises from correlations between different measurements. Surveys covering overlapping sky areas will exhibit correlated cosmic variance contributions. Different analyses of the same raw data (e.g., varying analysis choices within a single survey collaboration) are even more strongly correlated. Throughout this review, we identify cases where measurements are derived from the same underlying data and should not be treated as independent constraints.

The joint analysis of KiDS and DES data by Abbott *et al.* (2023) represents an important step toward properly accounting for such correlations when combining constraints from different surveys.

3 The Combined CMB Baseline: Technical Details

3.1 Component Datasets

The Combined CMB baseline integrates three primary datasets, each contributing distinct information about the primordial universe.

3.1.1 Planck 2018

The *Planck* satellite observed the CMB in nine frequency bands spanning 30–857 GHz, enabling robust separation of the CMB signal from Galactic and extragalactic foregrounds. The 2018 legacy data release (Planck Collaboration *et al.*, 2020) includes temperature (TT) and polarization (TE, EE) power spectra spanning multipoles $2 \leq \ell \leq 2500$ for temperature and $2 \leq \ell \leq 2000$ for polarization. The low- ℓ likelihood ($\ell < 30$) constrains the optical depth to reionization τ , which is partially degenerate with A_s (the amplitude of primordial scalar perturbations) and hence affects σ_8 inference. The high- ℓ likelihood constrains the shape and amplitude of the acoustic peaks, providing sensitivity to Ω_m , $\Omega_b h^2$, H_0 , and n_s .

Under the assumption of flat Λ CDM with minimal neutrino mass ($\sum m_\nu = 0.06$ eV), *Planck* 2018 alone yields $S_8 = 0.832 \pm 0.013$ (Planck Collaboration *et al.*, 2020).

3.1.2 ACT Data Release 6

The Atacama Cosmology Telescope is a 6-meter telescope located in the Atacama Desert of Chile at an elevation of 5190 meters. Its high angular resolution (approximately 1.4 arcminutes at 150 GHz) enables precise measurements of the CMB damping tail at $\ell > 2000$, where *Planck*'s beam dilutes the signal. ACT DR6 (Louis *et al.*, 2025) includes temperature and polarization power spectra from observations conducted between 2017 and 2022, with maps covering approximately 45% of the sky ($\sim 19\,000 \text{ deg}^2$) of which $\sim 25\%$ is used for the power spectrum analysis after masking the Galactic plane and bright extragalactic sources.

The damping tail measurements are particularly valuable for constraining the effective number of relativistic species N_{eff} and the primordial helium abundance Y_p , parameters that affect the shape of the power spectrum at small scales. ACT DR6 also provides an independent measurement of CMB lensing (Madhavacheril *et al.*, 2024), which directly probes the integrated matter distribution along the line of sight and yields constraints on S_8 that are complementary to the primary CMB anisotropies.

3.1.3 SPT-3G

The South Pole Telescope is a 10-meter telescope located at the Amundsen-Scott South Pole Station. Its location provides exceptional atmospheric stability, enabling deep integrations over a contiguous 1500 deg^2 survey field. SPT-3G, the third-generation camera, employs approximately 16,000 polarization-sensitive bolometers operating at 95, 150, and 220 GHz.

SPT-3G (Camphuis *et al.*, 2025) contributes high signal-to-noise measurements of the E-mode polarization power spectrum and provides the most precise ground-based measurements of the damping tail at $\ell > 3000$. The combination of SPT-3G with *Planck* and ACT yields improved constraints on parameters affecting the high- ℓ spectrum, including the damping scale and the amplitude of gravitational lensing of the CMB.

3.2 Combination Methodology

The combination of *Planck*, ACT, and SPT data requires careful treatment of several effects. Different experiments observe overlapping regions of sky, introducing covariance between their measurements due to shared cosmic variance. This covariance must be properly modeled to avoid underestimating parameter uncertainties. Additionally, each experiment employs distinct foreground models, beam characterization procedures, and calibration strategies. Joint analyses must either marginalize over inter-experiment calibration differences or demonstrate consistency when adopting unified calibration.

The Combined CMB analysis presented in association with DES Y6 (Abbott *et al.*, 2026) employs a likelihood that accounts for cross-correlations between experiments while marginalizing

over residual calibration uncertainties. The resulting constraint $S_8 = 0.836^{+0.012}_{-0.013}$ is robust to reasonable variations in analysis choices.

An independent but related constraint comes from CMB lensing. The combined ACT, SPT, and *Planck* lensing analysis (Qu *et al.*, 2026) constructs a joint Gaussian likelihood from the CMB lensing bandpowers of ACT DR6, *Planck* PR4, and SPT-3G. When supplemented with DESI DR2 BAO data to break the degeneracy between σ_8 and Ω_m , they obtain a competitive constraint on the parameter combination best measured by cosmic shear, $S_8 \equiv \sigma_8(\Omega_m/0.3)^{0.5} = 0.828 \pm 0.012$. This CMB lensing constraint probes the matter distribution at intermediate redshifts ($z \approx 0.9\text{--}5$) and provides an important bridge between the recombination epoch and the late universe probed by galaxy surveys.

4 Late-Universe Probes: Physical Principles and Systematic Uncertainties

4.1 Weak Gravitational Lensing

Weak gravitational lensing refers to the coherent distortion of background galaxy images by intervening large-scale structure. The observable quantity is the cosmic shear field γ , which can be decomposed into E-mode and B-mode components analogous to CMB polarization. In the absence of systematic effects, cosmological lensing produces only E-modes; non-zero B-modes indicate residual systematics from PSF modeling, detector effects, or other sources.

The cosmic shear two-point correlation function (or equivalently, the shear power spectrum) is related to the matter power spectrum through a weighted projection:

$$C_\ell^{ij} = \int_0^{\chi_H} d\chi \frac{W^i(\chi)W^j(\chi)}{\chi^2} P\left(\frac{\ell + 1/2}{\chi}, z(\chi)\right), \quad (4)$$

where $W^i(\chi)$ is the lensing efficiency kernel for source redshift bin i , χ is the comoving distance, and $P(k, z)$ is the nonlinear matter power spectrum. The Limber approximation has been employed here, which is accurate for $\ell \gtrsim 10$.

The dependence on S_8 enters primarily through the amplitude of the matter power spectrum, while the shape of the shear correlation function constrains the combination of Ω_m and the spectral index n_s . The characteristic degeneracy direction in the $\sigma_8\text{--}\Omega_m$ plane arises from the geometric weighting by the lensing kernels, which are sensitive to both the amplitude and redshift distribution of source galaxies.

4.1.1 Systematic Uncertainties in Cosmic Shear

Several systematic effects can bias cosmic shear measurements and hence S_8 inference. These have been extensively discussed in the context of DES (Yamamoto *et al.*, 2025), KiDS (Wright *et al.*, 2025; Li *et al.*, 2023), and HSC (Dalal *et al.*, 2023; Hikage *et al.*, 2019).

Shear measurement bias: The shear field must be estimated from noisy galaxy images with complex morphologies. Multiplicative biases m (defined such that the estimated shear $\hat{\gamma} = (1 + m)\gamma^{\text{true}}$) directly propagate to S_8 as $\Delta S_8/S_8 \approx m$. Current surveys aim for $|m| < 0.01$, but achieving this requires sophisticated calibration using image simulations that accurately reproduce the properties of observed galaxies. The DES Y6 analysis employs the METADETECTION algorithm (Yamamoto *et al.*, 2025), which achieves multiplicative bias uncertainties below 0.5%.

Photometric redshift errors: Cosmic shear analyses rely on photometric redshifts to assign galaxies to tomographic bins. Biases in the mean redshift of each bin shift the inferred S_8 , with typical sensitivities of $\Delta S_8/\Delta\langle z \rangle \approx -0.4 S_8$ per bin. The KiDS-Legacy analysis (Wright *et al.*, 2025) employs a sophisticated self-organizing map (SOM) methodology combined with

spectroscopic calibration samples to achieve redshift distribution uncertainties at the sub-percent level in mean redshift.

Intrinsic alignments: Galaxies are not randomly oriented tracers of the shear field; they are physically connected to the large-scale structure in which they form. Tidal interactions with the surrounding density field induce coherent alignments that mimic the cosmic shear signal. These contributions manifest as two distinct terms: “intrinsic-intrinsic” (II) correlations, arising between physically close galaxies aligned with the same local tidal field, and “gravitational-intrinsic” (GI) correlations, which occur when a foreground structure aligns a foreground galaxy while simultaneously lensing a background galaxy. The physical origin of these alignments depends on galaxy type: pressure-supported elliptical (red) galaxies are primarily aligned through tidal stretching, a mechanism well-described by the Nonlinear Alignment (NLA) model. In contrast, angular-momentum-supported spiral (blue) galaxies are influenced by tidal torquing, which requires higher-order descriptions such as the Tidal Alignment and Tidal Torquing (TATT) model utilized in recent analyses like DES Y6. Unmodeled IA typically suppresses the observed shear signal (dominated by the negative GI term), potentially biasing inferred S_8 values low if not properly accounted for. However, the choice of IA model involves a critical trade-off: while simple models like NLA may be insufficient for deep surveys mixing galaxy populations, highly flexible models like TATT introduce broad priors that can degrade constraining power and potentially absorb non-IA physical signals, such as baryonic suppression.

Baryon feedback: The nonlinear matter power spectrum is modified on small scales ($k > 1 h \text{ Mpc}^{-1}$) by baryonic processes including gas cooling, star formation, and AGN feedback. The FLAMINGO hydrodynamical simulations (Schaye *et al.*, 2023; McCarthy *et al.*, 2023) have demonstrated that these effects can suppress power by up to 20–30% at $k \sim 10 h \text{ Mpc}^{-1}$, potentially biasing S_8 constraints if not properly accounted for. Current cosmic shear analyses marginalize over feedback uncertainties using parameterized models calibrated against simulations.

4.2 Galaxy Clustering and the 3×2pt Framework

Galaxy clustering measurements probe the matter distribution through the positions of galaxies, which trace the underlying density field with a bias b that depends on galaxy type, luminosity, and redshift. The galaxy angular power spectrum C_ℓ^{gg} is related to the matter power spectrum by:

$$C_\ell^{gg,ij} = \int d\chi \frac{n^i(\chi)n^j(\chi)}{\chi^2} b^i(z)b^j(z) P\left(\frac{\ell+1/2}{\chi}, z\right), \quad (5)$$

where $n^i(\chi)$ is the comoving number density distribution of lens galaxies in bin i .

The combination of cosmic shear, galaxy clustering, and galaxy-galaxy lensing (the cross-correlation between lens positions and source shears) constitutes the “3 × 2pt” analysis framework employed by DES (Abbott *et al.*, 2026, 2022) and KiDS (Heymans *et al.*, 2021). This combination is powerful because it enables self-calibration of galaxy bias and provides complementary constraints on cosmological parameters. The galaxy-galaxy lensing signal depends on the product of galaxy bias and the matter amplitude, breaking degeneracies present in either probe alone.

Recent analyses combining galaxy-galaxy lensing with spectroscopic surveys have yielded particularly interesting results. Luo *et al.* (2025) find $S_8 = 0.8294 \pm 0.0110$ from HSC lensing combined with BOSS spectroscopy, in excellent agreement with the CMB baseline and suggesting that the low S_8 values from some cosmic shear analyses may reflect systematic effects rather than new physics.

4.3 Galaxy Cluster Counts

The abundance of galaxy clusters as a function of mass and redshift provides a sensitive probe of the growth of structure. The halo mass function dn/dM depends exponentially on σ_8 at the high-mass end, making cluster counts particularly sensitive to the clustering amplitude. The observable-mass relation (connecting X-ray luminosity, SZ signal, or richness to true mass) represents the primary systematic uncertainty in cluster cosmology. The mass-richness relation (for optical clusters) or hydrostatic bias (for X-ray/SZ) are the specific dominant nuisance parameters driving the uncertainties.

Multiple cluster analyses have contributed to the S_8 landscape in recent years. Ghirardini *et al.* (2024) present X-ray cluster cosmology from the eROSITA All-Sky Survey, finding $S_8 = 0.86 \pm 0.01$ —notably higher than other late-universe probes, though the discrepancy stands at only 1.5σ . In contrast, SPT cluster analyses (Bocquet *et al.*, 2024) favor lower values ($S_8 \approx 0.79$ – 0.80), creating an internal tension within cluster cosmology that remains unresolved. Earlier analyses combining *Planck* SZ clusters with various mass calibration approaches have yielded S_8 values consistent with or lower than the SPT results, rather than intermediate between SPT and eROSITA. Zubeldia and Challinor (2019), using CMB lensing mass calibration, report $\sigma_8 = 0.76 \pm 0.04$ and $\Omega_m = 0.33 \pm 0.02$, corresponding to $S_8 \approx 0.80 \pm 0.05$ ¹. Aymerich *et al.* (2024), using Chandra X-ray and CFHT weak-lensing mass calibration, find $S_8 = 0.78 \pm 0.02$ for their baseline self-similar redshift evolution model and $S_8 = 0.81 \pm 0.02$ when the redshift evolution is left free. These values cluster around or below the SPT result ($S_8 \approx 0.80$), reinforcing a pattern of low S_8 from SZ cluster number counts and highlighting the discrepancy with the eROSITA value of $S_8 = 0.86 \pm 0.01$.

4.4 Redshift-Space Distortions

The peculiar velocities of galaxies induce anisotropies in the observed clustering pattern when distances are inferred from redshifts. These redshift-space distortions (RSD) provide a direct measurement of the growth rate $f\sigma_8$, where $f \equiv d \ln D / d \ln a$ is the logarithmic growth rate and D is the linear growth factor.

RSD measurements have been extensively used to probe the S_8 tension. Nunes and Vagnozzi (2021) combined RSD data with geometrical measurements from BAO and Type Ia supernovae to arbitrate between early- and late-universe determinations of S_8 , finding $S_8 = 0.762^{+0.030}_{-0.025}$ and concluding that there are hints, but no strong evidence yet, for suppressed growth relative to *Planck*. Benisty (2021) quantified the tension using RSD data alone, finding $S_8 = 0.700^{+0.038}_{-0.037}$ from Bayesian analysis, corresponding to a 3.2σ discrepancy with *Planck* (3.5σ relative to the Combined CMB baseline adopted in this review), while a model-independent Gaussian Process reconstruction yielded $S_8 \approx 0.70$ – 0.73 with the tension reduced to $\sim 1.5\sigma$ due to the larger uncertainties of the non-parametric approach. More recent analyses incorporating DESI full-shape clustering measurements, which include RSD information and constrain $\sigma_8 = 0.842 \pm 0.034$ (Adame *et al.*, 2025), and joint RSD+CMB fits (Sabogal *et al.*, 2024) continue to probe the consistency of growth rates with Λ CDM predictions.

The studies by Adil *et al.* (2024) and Akarsu *et al.* (2025) present an intriguing finding: S_8 appears to increase with effective redshift when inferred from different probes, potentially indicating scale-dependent or time-dependent modifications to structure formation within Λ CDM cosmology.

¹Derived from the reported σ_8 and Ω_m values using the standard definition $S_8 \equiv \sigma_8 \sqrt{\Omega_m/0.3}$. The original paper reports the combination $\sigma_8 (\Omega_m/0.33)^{0.25} = 0.765 \pm 0.035$ as its best-constrained parameter.

5 Compilation of S_8 Measurements (2019–2026)

5.1 Visual Summary

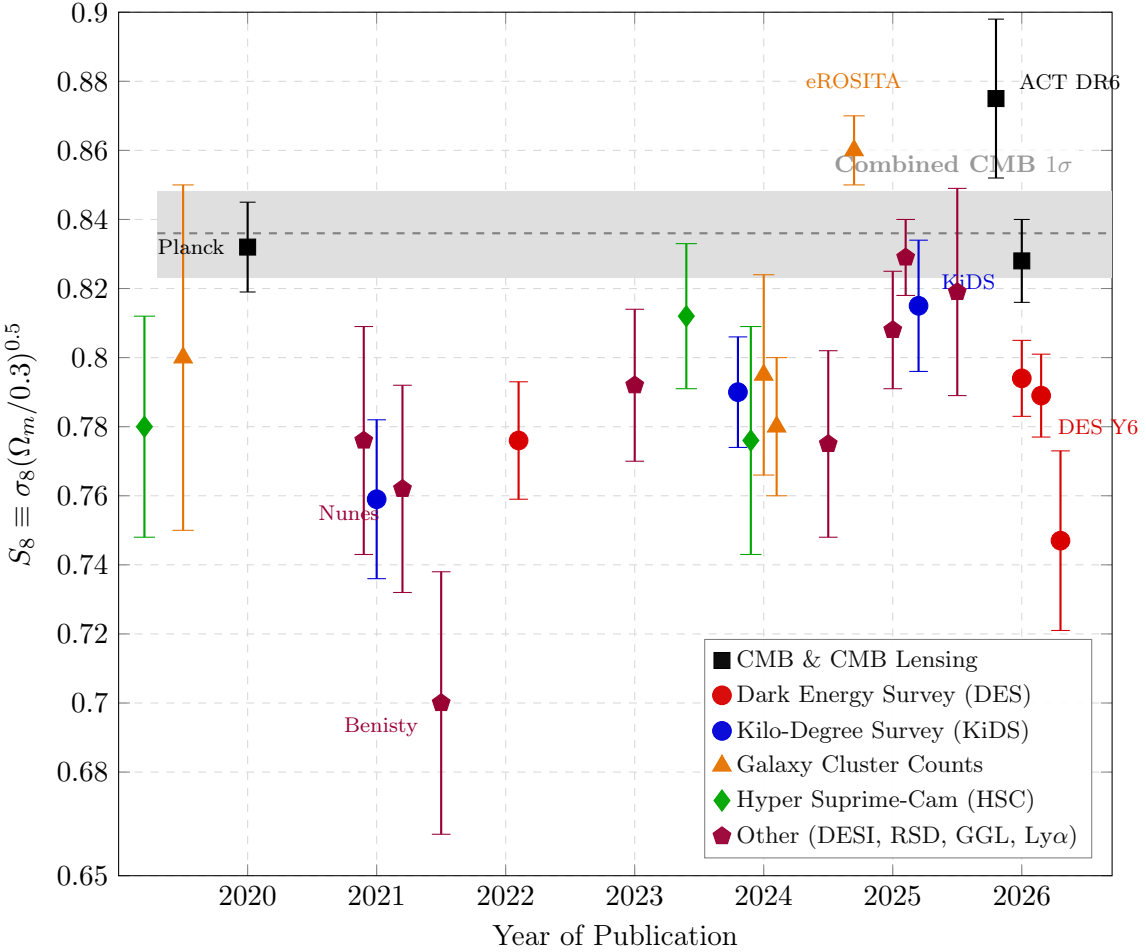


Figure 1: Compilation of S_8 measurements from major cosmological surveys (2019–2026). The horizontal gray band represents the 1σ confidence interval of the Combined CMB baseline (Planck + ACT DR6 + SPT-3G), centered at $S_8 = 0.836$ with asymmetric width $^{+0.012}_{-0.013}$. The dashed gray line indicates the central value. Note the systematic offset between DES results (red circles), which lie consistently below the CMB band, and KiDS Legacy results (blue circles), which have migrated upward into consistency with the CMB. The eROSITA cluster count measurement (orange triangle, upper region) uniquely favors a clustering amplitude exceeding the CMB baseline. Error bars represent 1σ uncertainties.

Several features are immediately apparent from this visualization. The DES measurements (red points) lie systematically below the CMB band across all data releases, with the Y6 results representing the most precise low- S_8 determination to date. In contrast, the KiDS results (blue points) show significant evolution: the KiDS-1000 result from 2021 (Asgari *et al.*, 2021) exhibited a pronounced tension similar to DES, but the KiDS Legacy result from 2025 (Wright *et al.*, 2025) has shifted upward into consistency with the CMB. The eROSITA cluster count measurement (Ghirardini *et al.*, 2024) stands out as the sole late-universe probe favoring S_8 values above the CMB baseline.

The spectroscopic and RSD probes (purple pentagons) span a notably wide range, from $S_8 = 0.700$ (Benisty, 2021) to $S_8 = 0.829$ (Luo *et al.*, 2025), reflecting the diversity of methodologies within this category. Galaxy cluster counts (orange triangles) exhibit striking internal

disagreement, with eROSITA favouring S_8 above the CMB band while SPT and Planck SZ clusters fall well below. Galaxy-galaxy lensing and peculiar velocity measurements cluster near the CMB baseline, suggesting consistency when weak lensing systematics are avoided.

5.2 Detailed Tabulation

Table 1 provides comprehensive information for each measurement, including the probe type, publication date, S_8 value with uncertainties, tension level relative to the Combined CMB baseline, and relevant citations.

Table 1: Comprehensive compilation of S_8 measurements and their tension with the Combined CMB baseline ($S_8 = 0.836^{+0.012}_{-0.013}$). Tensions are computed using the uncertainty in the direction of the discrepancy for asymmetric errors.

Probe / Analysis	Date	S_8 Value	Tension	Reference & Notes
CMB & Early Universe Baselines				
Combined CMB	Jan 2026	$0.836^{+0.012}_{-0.013}$	—	Planck+ACT+SPT; primary baseline (Abbott <i>et al.</i> , 2026)
Combined Lensing	Jan 2026	0.828 ± 0.012	0.5σ	ACT+SPT+ <i>Planck</i> lensing + DESI DR2 BAO (Qu <i>et al.</i> , 2026)
ACT DR6 (primary CMB)	Nov 2025	0.875 ± 0.023	1.5σ	ACT DR6 power spectra alone (+ Sroll2 τ prior); above baseline (Louis <i>et al.</i> , 2025)
Planck 2018	Sep 2020	0.832 ± 0.013	—	Previous baseline (Planck Collaboration <i>et al.</i> , 2020)
Dark Energy Survey				
DES Y6 (All)	Jan 2026	$0.794^{+0.009}_{-0.012}$	2.4σ	$3 \times 2\text{pt} + \text{BAO} + \text{SNe} + \text{clusters}$ (Abbott <i>et al.</i> , 2026)
DES Y6 ($3 \times 2\text{pt}$)	Jan 2026	0.789 ± 0.012	2.7σ	$3 \times 2\text{pt}$ analysis (cosmic shear + galaxy clustering + galaxy-galaxy lensing) (Abbott <i>et al.</i> , 2026)
DES Y6 (Shear)	Jan 2026	$0.783^{+0.019}_{-0.015}$	2.7σ	Cosmic shear only (Abbott <i>et al.</i> , 2026)
DES Y6 ($w\text{CDM}$)	Jan 2026	$0.781^{+0.021}_{-0.020}$	1.1σ	Extended model; reported tension (Abbott <i>et al.</i> , 2026)
DES Y3 ($3 \times 2\text{pt}$)	Jan 2022	0.776 ± 0.017	2.8σ	Previous DES release (Abbott <i>et al.</i> , 2022)
DES Y1 ($3 \times 2\text{pt}$)	Jan 2026	$0.747^{+0.027}_{-0.025}$	3.2σ	Reanalysis with Y6 pipeline (Abbott <i>et al.</i> , 2026)
Kilo-Degree Survey				
KiDS-Legacy (Shear)	Mar 2025	$0.815^{+0.016}_{-0.021}$	0.9σ	Final KiDS result (Wright <i>et al.</i> , 2025)

Continued on next page...

Probe / Analysis	Date	S_8 Value	Tension	Reference & Notes
KiDS-1000 + DES Y3	Oct 2023	$0.790^{+0.018}_{-0.014}$	2.4σ	Joint cosmic shear analysis (Abbott <i>et al.</i> , 2023)
KiDS-1000 (Shear)	Jan 2021	$0.759^{+0.024}_{-0.021}$	3.1σ	Superseded (Asgari <i>et al.</i> , 2021)
Hyper Suprime-Cam				
HSC Y3 (Shear)	Dec 2023	$0.776^{+0.032}_{-0.033}$	1.7σ	Third-year analysis (Dalal <i>et al.</i> , 2023)
HSC Y1 (Unified)	Apr 2023	0.812 ± 0.021	1.0σ	Unified pipeline (Longley <i>et al.</i> , 2023)
HSC Y1 (Original)	Mar 2019	$0.780^{+0.030}_{-0.033}$	1.6σ	Original analysis (Hikage <i>et al.</i> , 2019)
Galaxy Cluster Counts				
eROSITA (X-ray)	Oct 2024	0.860 ± 0.010	-1.5σ	Higher than CMB (Ghirardini <i>et al.</i> , 2024)
SPT-3G Clusters	Jan 2024	0.795 ± 0.029	1.3σ	SZ-selected (Bocquet <i>et al.</i> , 2024)
<i>Planck</i> SZ (Chandra+WL)	Feb 2024	0.780 ± 0.020	2.3σ	PSZ2 cluster counts, Chandra X-ray + CFHT WL mass calibration (Aymerich <i>et al.</i> , 2024)
<i>Planck</i> +CMB lensing	2019	0.80 ± 0.05^1	0.7σ	Lensing mass calibration (Zubeldia and Challinor, 2019)
Spectroscopic & Other Probes				
GGL (HSC×BOSS)	Feb 2025	0.8294 ± 0.0110	0.4σ	Galaxy-galaxy lensing (Luo <i>et al.</i> , 2025)
DESI DR1 + Lensing	May 2025	0.808 ± 0.017	1.3σ	3D clustering + CMB lensing (Maus <i>et al.</i> , 2025)
Peculiar Velocities	Sep 2025	0.819 ± 0.030	0.5σ	TFR+FP+SNe joint (Stiskalek, 2025)
RSD compilation	Aug 2024	0.775 ± 0.027	2.0σ	RSD+DESI+PP (Sabogal <i>et al.</i> , 2024)
BOSS Full-Shape	2023	0.792 ± 0.022	1.7σ	Clustering + GGL (Lange <i>et al.</i> , 2023)
RSD (Benisty)	2021	$0.700^{+0.038}_{-0.037}$	3.5σ	RSD compilation (Benisty, 2021)
RSD+BAO+SNe	2021	$0.762^{+0.030}_{-0.025}$	2.3σ	RSD compilation + BAO + SNeIa (Nunes and Vagnozzi, 2021)
Ly α Forest	Nov 2020	0.776 ± 0.033^2	1.7σ	SDSS DR14 (Palanque-Delabrouille <i>et al.</i> , 2020)

6 Analysis of Key Results

6.1 The Dark Energy Survey Year 6 Analysis

The DES Year 6 (Y6) analysis (Abbott *et al.*, 2026) represents the culmination of the Dark Energy Survey’s imaging program, utilizing the full six years of observations collected with the Dark Energy Camera on the 4-meter Blanco telescope at Cerro Tololo Inter-American Observatory. The Y6 dataset encompasses approximately 5000 deg^2 of the southern sky, reaching limiting magnitudes of $g \approx 24.7$, $r \approx 24.4$, $i \approx 23.8$, and $z \approx 23.0$ (10σ point source).

6.1.1 Methodological Advances

The Y6 analysis incorporates several methodological improvements relative to the Y3 release (Abbott *et al.*, 2022). The shear catalog employs the METADETECTION algorithm (Yamamoto *et al.*, 2025), an evolution of METACALIBRATION that uses image manipulations to mitigate detection and shear measurement biases. However, the analysis explicitly utilizes a suite of image simulations to characterize galaxy blending and determine priors for the multiplicative shear bias. This approach achieves multiplicative bias uncertainties ranging from approximately 0.6% to 1.2%.

The photometric redshift distributions are calibrated using a hybrid framework that combines the Self-Organizing Map $n(z)$ method (SOMPZ), which maps spectroscopic information from deep fields to the wide survey using transfer functions from image simulations, with clustering-redshift cross-correlations (WZ) against spectroscopic samples (Abbott *et al.*, 2026). The intrinsic alignment model employs the tidal alignment and tidal torquing (TATT) framework, marginalizing over amplitude and redshift-evolution parameters (A_1, A_2, η_1, η_2) using informative priors on the evolution terms motivated by observations, while holding the tidal alignment bias parameter b_{TA} fixed (Abbott *et al.*, 2026).

6.1.2 Results and Tension Assessment

The DES Y6 $3 \times 2\text{pt}$ analysis yields $S_8 = 0.789 \pm 0.012$, representing a 2.6σ tension with the Combined CMB baseline in the S_8 projection. This tension remains consistent when comparing to the cosmic shear signal alone, which favors an even lower value of $S_8 = 0.783^{+0.019}_{-0.015}$, suggesting that the tension is not an artifact of galaxy bias modeling in the clustering and galaxy-galaxy lensing components.

The combination of DES Y6 $3 \times 2\text{pt}$ with other internal DES probes (DES BAO, DES Supernovae, and DES Cluster Counts) yields the tightest internal constraint, $S_8 = 0.794^{+0.009}_{-0.012}$. This combined result exhibits a 2.8σ tension with the Combined CMB in the full parameter space.

6.1.3 Extended Cosmological Models

When the dark energy equation of state parameter w is allowed to vary freely, the DES Y6 constraint shifts to $S_8 = 0.781^{+0.021}_{-0.020}$, reducing the tension with the Combined CMB to 1.3σ in the full parameter space (1.0σ when projected onto S_8) (Abbott *et al.*, 2026). While the measurement yields a central value of $w = -1.12^{+0.26}_{-0.20}$ lying in the phantom regime, the results show no statistically significant preference for $w \neq -1$ (finding only a 0.9σ preference for $w\text{CDM}$ over ΛCDM), distinguishing these findings from the hints of dynamical dark energy reported in DESI BAO measurements (Abdul Karim *et al.*, 2025).

²Derived from the reported $\sigma_8 = 0.811 \pm 0.024$ and $\Omega_m = 0.275 \pm 0.012$ using $S_8 \equiv \sigma_8 \sqrt{\Omega_m/0.3}$.

6.2 Evolution from KiDS-1000 to Legacy

The most striking aspect of the KiDS Legacy results is the substantial upward shift in S_8 relative to KiDS-1000 (Asgari *et al.*, 2021). The KiDS-1000 analysis reported $S_8 = 0.759^{+0.024}_{-0.021}$, exhibiting a $\sim 3\sigma$ tension with both *Planck* and the Combined CMB. The KiDS Legacy result, $S_8 = 0.815^{+0.016}_{-0.021}$, represents an increase of $\Delta S_8 = 0.056$, or approximately 2.3σ in the KiDS-1000 error budget.

As discussed by Wright *et al.* (2025), this shift primarily results from improved redshift distribution estimation and calibration, as well as an expanded survey area and improved image reduction. These advances were enabled in large part by the SKiLLS multi-band image simulations (Li *et al.*, 2023), which provided the first joint shear and redshift calibration for KiDS through realistic nine-band simulated imaging, refined PSF modelling, and improved treatment of blending effects across different redshifts.

6.2.1 Implications for the Tension Landscape

The joint analysis by Abbott *et al.* (2023) represents an important attempt to address these discrepancies through consistent analysis choices. By applying a unified methodology to both KiDS-1000 and DES Y3 cosmic shear data, they find $S_8 = 0.790^{+0.018}_{-0.014}$, a value that lies above both individual survey results, suggesting that harmonised analysis choices can shift S_8 estimates upward relative to each survey’s default pipeline.

6.3 The eROSITA Cluster Count Anomaly

The eROSITA (extended ROentgen Survey with an Imaging Telescope Array) X-ray telescope has yielded one of the most surprising results in the S_8 landscape. Ghirardini *et al.* (2024) report $S_8 = 0.860 \pm 0.010$ from the eRASS1 cluster sample in the western Galactic hemisphere—notably *higher* than the Combined CMB baseline, though the discrepancy stands at only 1.5σ .

6.3.1 Physical Interpretation

The eROSITA result stands apart from other late-universe probes in its direction: rather than indicating less structure than predicted by the CMB, the cluster counts favour a higher S_8 . If this trend persists with reduced uncertainties, it could point to issues with the observable-mass relation calibration used to convert X-ray luminosity to halo mass, or to scale-dependent modifications of gravity that enhance clustering on cluster scales.

6.3.2 Comparison with Other Cluster Samples

The tension between eROSITA and other cluster count analyses is difficult to explain within standard cosmological models. SPT clusters (Bocquet *et al.*, 2024), selected via the Sunyaev-Zel’dovich effect, favor $S_8 = 0.795 \pm 0.029$ —fully 2σ below eROSITA despite using a mass proxy that is largely independent of X-ray properties. Analyses of *Planck* SZ clusters yield similarly low values: Aymerich *et al.* (2024) find $S_8 = 0.780 \pm 0.020$ using Chandra X-ray and weak lensing mass calibration, while Zubeldia and Challinor (2019) report $S_8 = 0.80 \pm 0.05$ using CMB lensing mass calibration. The discrepancy between X-ray and SZ-selected cluster cosmology constraints suggests that sample selection effects, differences in mass calibration methods, or systematic differences in the cluster populations probed may be responsible.

6.4 Spectroscopic Probes: DESI and RSD Measurements

The Dark Energy Spectroscopic Instrument (DESI) is revolutionizing spectroscopic cosmology by obtaining redshifts for tens of millions of galaxies and quasars. The DESI Data Release 1 (DR1) cosmological analysis (DESI Collaboration *et al.*, 2025; Adame *et al.*, 2025) combines BAO

distance measurements, redshift-space distortion growth rate constraints, and cross-correlations with CMB lensing. The analysis by Maus *et al.* (2025) yields $S_8 = 0.808 \pm 0.017$, representing an intermediate value between the DES weak lensing results and the CMB baseline. The 1.3σ tension with the Combined CMB is not statistically significant, but the preference for lower S_8 values relative to the CMB is directionally consistent with most cosmic shear analyses. RSD measurements provide a direct probe of the growth rate $f\sigma_8$. The compilation by Sabogal *et al.* (2024) consistently favors growth rates approximately 5–10% lower than the Λ CDM prediction given CMB parameters, providing independent corroboration of suppressed late-time structure growth. Earlier pre-DESI compilations reached similar conclusions: Nunes and Vagnozzi (2021) report $S_8 = 0.762_{-0.025}^{+0.030}$ (2.3σ tension) from combined RSD, BAO, and SNeIa data, while Benisty (2021) find a notably lower $S_8 = 0.700_{-0.037}^{+0.038}$ (3.5σ tension).

6.5 Galaxy-Galaxy Lensing and Alternative Probes

An important cross-check comes from galaxy-galaxy lensing (GGL), which measures the tangential shear of background sources around foreground lens galaxies. Luo *et al.* (2025) combine HSC weak lensing with BOSS spectroscopic lenses to obtain $S_8 = 0.8294 \pm 0.0110$, in excellent agreement (0.4σ) with the CMB baseline. This result is particularly significant because it employs an independent methodology from the cosmic shear 3×2 pt analyses, yet finds no evidence for tension. Stiskalek (2025) present constraints from peculiar velocity surveys using Tully-Fisher relations, the Fundamental Plane, and Type Ia supernovae as distance indicators. Their joint analysis yields $S_8 = 0.819 \pm 0.030$, consistent with both the CMB and KiDS Legacy while being independent of weak lensing systematics entirely.

7 Systematic Effects: A Critical Assessment

7.1 Photometric Redshift Calibration

Photometric redshift errors represent one of the leading systematic uncertainties in cosmic shear analyses. The sensitivity of S_8 to mean redshift biases can be parameterized as:

$$\frac{\partial S_8}{\partial \Delta z_i} \approx -0.4 S_8 w_i, \quad (6)$$

where Δz_i is the bias in the mean redshift of tomographic bin i and w_i is the weight of that bin in the overall constraint. The photometric redshift calibration strategies employed by DES, KiDS, and HSC differ in important ways. DES relies primarily on the SOMPZ method, which uses self-organizing maps to create a mapping between photometric and spectroscopic samples. KiDS (Wright *et al.*, 2025) employs direct spectroscopic calibration supplemented by multi-band image simulations from SKILLS (Li *et al.*, 2023) for joint shear and redshift calibration. HSC uses a combination of clustering- z and photometric template fitting methods. These different approaches are sensitive to different potential biases. The evolution of KiDS from $S_8 \approx 0.76$ (KiDS-1000) to $S_8 \approx 0.82$ (Legacy) was driven primarily by improved redshift distribution estimation and calibration (Wright *et al.*, 2025), demonstrating the magnitude of potential systematic shifts.

7.2 Shear Measurement Systematics

The estimation of galaxy shapes from noisy, PSF-convolved images is a challenging inverse problem. The METADETECTION method used by DES (Yamamoto *et al.*, 2025) and the LENSFIT algorithm used by KiDS employ fundamentally different approaches to this problem. The unified catalogue-level reanalysis by Longley *et al.* (2023) provides a crucial test of analysis-level systematics. By applying a consistent analysis framework—unified cosmological priors, intrinsic alignment model, and small-scale treatment—to DES-Y1, HSC-Y1, and KiDS-1000, they find

that analysis choices can shift S_8 by $\sim 0.03\text{--}0.05$, comparable to the difference between DES and KiDS results.

7.3 Intrinsic Alignments

Intrinsic alignments (IA) represent a fundamental astrophysical contaminant in cosmic shear analyses. The amplitude and redshift evolution are typically parameterized using the nonlinear alignment (NLA) or tidal alignment and tidal torquing (TATT) models.

Current constraints on IA parameters from cosmic shear alone are weak. Amon and Efstathiou (2022) note that while intrinsic alignments are a potential solution, they find that fixing the IA amplitude to zero only exacerbates the tension for certain datasets. Instead, they argue that a suppression of the matter power spectrum on non-linear scales—potentially due to baryonic feedback or non-standard dark matter—is a more statistically favored explanation for the S_8 discrepancy than complex intrinsic alignment models.

7.4 Baryon Feedback and Nonlinear Modeling

The matter power spectrum on small scales is modified by baryonic processes that redistribute mass relative to dark matter-only predictions. The FLAMINGO hydrodynamical simulations (Schaye *et al.*, 2023; McCarthy *et al.*, 2023) have been instrumental in quantifying these effects, demonstrating that gas expulsion by AGN feedback can suppress the matter power spectrum by up to 20–30% at scales of $k \sim 1\text{--}10 \, h \, \text{Mpc}^{-1}$ (McCarthy *et al.*, 2023). Notably, McCarthy *et al.* (2023) find that while baryonic feedback significantly suppresses the power spectrum, simulations calibrated to observed cluster gas fractions and galaxy stellar mass functions do not resolve the S_8 tension, as they generally predict a suppression that is insufficient to reconcile weak lensing data with the Planck CMB baseline.

Cosmic shear analyses must account for these baryonic effects, either by restricting to large angular scales where the impact is minimal or by marginalizing over parameterized feedback models. The sensitivity of S_8 to baryonic feedback modeling is scale-dependent; analyses that extend to smaller angular scales are more sensitive to feedback uncertainties but gain statistical precision.

8 Theoretical Interpretations

8.1 Consistency within Λ CDM

Before invoking new physics, it is essential to evaluate whether the observed tension pattern can be explained within the standard Λ CDM framework. The heterogeneous nature of the current tension landscape—with DES and KiDS both favoring lower S_8 than the CMB but differing significantly from each other—suggests that systematic effects may play a significant role. If the true S_8 value lies near 0.815 (the KiDS Legacy result), then DES Y6 would require a downward systematic bias of approximately 0.025. Conversely, if the true value is near 0.789 (DES Y6), then KiDS Legacy would require an upward bias of similar magnitude. Neither scenario is implausible given the known systematic uncertainties in weak lensing analyses, as emphasized by Amon and Efstathiou (2022).

8.2 Modified Gravity

If the S_8 tension reflects genuine new physics, modifications to the gravitational sector represent a natural avenue for exploration. In general relativity, the growth of linear density perturbations δ is governed by:

$$\ddot{\delta} + 2H\dot{\delta} - 4\pi G\rho_m\delta = 0. \quad (7)$$

Scalar-tensor theories, such as $f(R)$ gravity (Hu and Sawicki, 2007), introduce a fifth force that can enhance or suppress structure growth depending on the screening mechanism employed. These models can in principle produce scale-dependent S_8 values that differ between CMB lensing (which probes $z \sim 2$) and galaxy surveys (which probe $z < 1$).

8.3 Interacting Dark Sector

Models in which dark matter interacts with dark energy can suppress the growth of structure at late times. Sabogal *et al.* (2024) find evidence for such interactions when combining RSD measurements with DESI and Planck data, though the significance depends on the specific interaction model considered.

The decay of a fraction of dark matter into dark radiation reduces the total matter density available to cluster, lowering σ_8 relative to Λ CDM. Tanimura *et al.* (2023) have tested such models using the thermal Sunyaev-Zel'dovich effect, finding that decaying dark matter can partially alleviate the tension.

8.4 Evolving Dark Energy

The DESI BAO results (DESI Collaboration *et al.*, 2025) have generated significant interest by suggesting a potential preference for evolving dark energy ($w \neq -1$). As noted in the DES Y6 analysis, allowing w to vary reduces the S_8 tension from 2.6σ to $\sim 1\sigma$.

If confirmed, evolving dark energy would represent a fundamental departure from Λ CDM. However, while the DES Y6 data yield a central value of $w = -1.12$ (in the "phantom" regime, $w < -1$), they show no statistically significant preference for w CDM over Λ CDM (0.9σ), contrasting with the stronger hints ($> 3\sigma$) reported in DESI BAO combinations. Confirmation from independent datasets and combined analyses remains essential.

9 Discussion and Future Outlook

9.1 Summary of the Current Tension Landscape

The S_8 tension in 2026 presents a complex and nuanced picture that defies simple characterization. The key findings of this review can be summarized as follows:

The baseline has shifted. The adoption of the Combined CMB (Planck + ACT + SPT) as the reference (Abbott *et al.*, 2026; Louis *et al.*, 2025; Camphuis *et al.*, 2025) raises the early-universe S_8 determination from 0.832 ± 0.013 to $0.836^{+0.012}_{-0.013}$, increasing the precision by approximately 8% and shifting the central value upward.

DES maintains a significant tension. The DES Y6 analysis (Abbott *et al.*, 2026), representing the most precise cosmic shear measurement to date, exhibits a 2.4σ – 2.7σ tension with the Combined CMB that cannot be dismissed as statistical fluctuation.

KiDS has converged with the CMB. The KiDS Legacy analysis (Wright *et al.*, 2025) shows a dramatic upward shift from KiDS-1000 (Asgari *et al.*, 2021), bringing the result into sub- 1σ consistency with the CMB baseline.

Cluster counts show internal tension. The discrepancy between eROSITA (Ghirardini *et al.*, 2024) (high S_8) and SPT (Bocquet *et al.*, 2024) (low S_8) cluster analyses exceeds 2σ and requires explanation.

Spectroscopic probes span a wide range. DESI (Maus *et al.*, 2025) favors S_8 only 1.3σ below the CMB, while RSD compilations (Sabogal *et al.*, 2024; Nunes and Vagnozzi, 2021; Benisty, 2021) report tensions ranging from 2.0σ to 3.5σ , providing stronger evidence for suppressed late-time growth.

9.2 Paths to Resolution

Several developments in the near future may clarify the situation:

Cross-survey joint analyses. The KiDS + DES joint analysis by Abbott *et al.* (2023) represents a first step toward harmonizing weak lensing results. Extension of this approach to include HSC and upcoming surveys could identify systematic differences.

Euclid space telescope. The Euclid mission (Euclid Collaboration *et al.*, 2022), launched in 2023, will provide systematics-limited cosmic shear constraints free from ground-based atmospheric effects, covering 15,000 deg² with space-based image quality.

CMB-S4. The next-generation CMB-S4 experiment will provide cosmic variance-limited measurements of CMB lensing over most of the sky, offering an independent early-universe S_8 constraint with different systematic profiles.

Improved theoretical modeling. Continued development of hydrodynamical simulations (Schaye *et al.*, 2023; McCarthy *et al.*, 2023) and intrinsic alignment models will reduce theoretical systematic uncertainties in cosmic shear interpretation.

9.3 Concluding Remarks

The S_8 tension remains one of the most intriguing anomalies in precision cosmology. The transition to the Combined CMB baseline has sharpened the target for late-universe probes while revealing unexpected divergences among measurements that were previously thought to be in agreement. The resolution of this tension—whether through identification of systematic effects or discovery of new physics—will require continued collaboration between observational, theoretical, and statistical communities.

The coming years, with data from Euclid, Roman, DESI, CMB-S4, and advanced simulations, promise to transform our understanding of structure formation and potentially reveal new physics beyond the standard cosmological model. Whatever the outcome, the S_8 tension has demonstrated the power of precision cosmology to probe the fundamental nature of the universe and the importance of systematic error control in an era of percent-level measurements.

References

T. M. C. Abbott *et al.* (DES), Preprint (2026), arXiv:2601.14559 [astro-ph.CO] .

A. H. Wright *et al.*, *Astronomy & Astrophysics* **703**, A158 (2025), arXiv:2503.19441 [astro-ph.CO] .

Planck Collaboration, N. Aghanim, *et al.*, *Astronomy & Astrophysics* **641**, A6 (2020), arXiv:1807.06209 [astro-ph.CO] .

A. Amon and G. Efstathiou, *MNRAS* **516**, 5355 (2022), arXiv:2206.11794 [astro-ph.CO] .

M. Asgari *et al.*, *Astronomy & Astrophysics* **645**, A104 (2021), arXiv:2007.15633 [astro-ph.CO] .

T. M. C. Abbott *et al.* (DES), *Physical Review D* **105**, 023520 (2022), arXiv:2105.13549 [astro-ph.CO] .

C. Hikage *et al.* (HSC), *PASJ* **71**, 43 (2019), arXiv:1809.09148 [astro-ph.CO] .

C. G. Boiza, M. Petronikolou, M. Bouhmadi-López, and E. N. Saridakis, “Addressing H_0 and S_8 tensions within $f(Q)$ cosmology,” (2025), arXiv:2505.18264 [astro-ph.CO] .

M. S. Souza, A. M. Barcelos, R. C. Nunes, O. Akarsu, and S. Kumar, *Universe* **11**, 2 (2025), arXiv:2501.18031 [astro-ph.CO] .

R. Terasawa, M. Takada, T. Kurita, and S. Sugiyama, “Late-time suppression of structure growth as a solution for the S_8 tension,” (2025), arXiv:2505.09176 [astro-ph.CO] .

W. Hu and I. Sawicki, Physical Review D **76**, 064004 (2007), arXiv:0705.1158 [astro-ph] .

H. Tanimura, M. Douspis, N. Aghanim, and J. Kuruvilla, Astronomy & Astrophysics **674**, A222 (2023), arXiv:2301.03939 [astro-ph.CO] .

M. A. Sabogal *et al.*, Physical Review D **110**, 123508 (2024), arXiv:2408.12403 [astro-ph.CO] .

T. Louis *et al.* (Atacama Cosmology Telescope), JCAP **11**, 062 (2025), arXiv:2503.14452 [astro-ph.CO] .

E. Camphuis *et al.* (SPT-3G), “SPT-3G D1: CMB temperature and polarization power spectra and cosmology from 2019 and 2020 observations of the SPT-3G Main field,” (2025), arXiv:2506.20707 [astro-ph.CO] .

M. S. Madhavacheril *et al.* (ACT), Astrophys. J. **962**, 113 (2024), arXiv:2304.05203 [astro-ph.CO]

W. Handley and P. Lemos, Physical Review D **100**, 043504 (2019), arXiv:1902.04029 [astro-ph.CO] .

T. Tröster, A. G. Sánchez, M. Asgari, C. Blake, M. Crocce, C. Heymans, H. Hildebrandt, B. Joachimi, S. Joudaki, A. Kannawadi, C.-A. Lin, and A. Wright, Astronomy & Astrophysics **633**, L10 (2020), arXiv:1909.11006 [astro-ph.CO] .

T. M. C. Abbott *et al.* (Kilo-Degree Survey, DES), Open J. Astrophys. **6**, 2305.17173 (2023), arXiv:2305.17173 [astro-ph.CO] .

F. J. Qu *et al.* (ACT, SPT-3G), Phys. Rev. Lett. **136**, 021001 (2026), arXiv:2504.20038 [astro-ph.CO] .

M. Yamamoto *et al.*, Mon. Not. Roy. Astron. Soc. **543**, 4156 (2025), arXiv:2501.05665 [astro-ph.CO] .

S.-S. Li *et al.*, Astron. Astrophys. **670**, A100 (2023), arXiv:2210.07163 [astro-ph.CO] .

R. Dalal *et al.* (HSC), Physical Review D **108**, 123519 (2023), arXiv:2304.00701 [astro-ph.CO] .

J. Schaye, R. Kugel, M. Schaller, J. C. Helly, J. Braspennning, W. Elbers, I. G. McCarthy, M. P. van Daalen, B. Vandenbroucke, C. S. Frenk, J. Kwan, J. Salcido, Y. M. Bahé, J. Borrow, E. Chaikin, O. Hahn, F. Huško, A. Jenkins, C. G. Lacey, and F. S. J. Nobels, Monthly Notices of the Royal Astronomical Society **526**, 4978 (2023), arXiv:2306.04024 [astro-ph.CO] .

I. G. McCarthy *et al.*, Mon. Not. Roy. Astron. Soc. **526**, 5494 (2023), arXiv:2309.07959 [astro-ph.CO] .

C. Heymans, T. Tröster, M. Asgari, C. Blake, H. Hildebrandt, B. Joachimi, K. Kuijken, C.-A. Lin, A. G. Sánchez, J. L. van den Busch, A. H. Wright, A. Amon, M. Bilicki, J. de Jong, M. Crocce, A. Dvornik, T. Erben, M. C. Fortuna, F. Getman, B. Giblin, K. Glazebrook, H. Hoekstra, S. Joudaki, A. Kannawadi, C. Lidman, L. Miller, N. R. Napolitano, R. Poulton, M. Radovich, P. Schneider, H. Shan, C. Sifón, D. J. B. Smit, E. Tempel, and C. Wolf, Astronomy & Astrophysics **649**, A88 (2021), arXiv:2007.15632 [astro-ph.CO] .

X. Luo, K. Xu, Y. Jing, H. Gao, H. Li, D. Zhao, J. Han, C. Wei, and Y. Luo, “Photometric objects around cosmic webs (pac) delineated in a spectroscopic survey. viii. revisiting the lensing is low effect,” (2025), arXiv:2502.09404 [astro-ph.CO] .

V. Ghirardini *et al.*, *Astronomy & Astrophysics* **689**, A298 (2024), arXiv:2402.08458 [astro-ph.CO] .

S. Bocquet *et al.*, *Physical Review D* **110**, 083510 (2024), arXiv:2401.02075 [astro-ph.CO] .

Í. Zubeldia and A. Challinor, *MNRAS* **489**, 401 (2019), arXiv:1904.07887 [astro-ph.CO] .

G. Aymerich, M. Doussis, G. W. Pratt, L. Salvati, E. Sourié, F. Andrade-Santos, W. R. Forman, C. Jones, N. Aghanim, R. Kraft, and R. J. van Weeren, *A&A* **694**, A252 (2024), arXiv:2402.04006 [astro-ph.CO] .

R. C. Nunes and S. Vagnozzi, *MNRAS* **505**, 5427 (2021), arXiv:2106.01208 [astro-ph.CO] .

D. Benisty, *Physics of the Dark Universe* **31**, 100766 (2021), arXiv:2005.03751 [astro-ph.CO] .

A. G. Adame *et al.* (DESI), *JCAP* **01**, 124 (2025), arXiv:2404.03001 [astro-ph.CO] .

S. A. Adil, O. Akarsu, M. Malekjani, E. Ó Colgáin, S. Pourojaghi, A. A. Sen, and M. M. Sheikh-Jabbari, *Monthly Notices of the Royal Astronomical Society: Letters* **528**, L20 (2024), arXiv:2303.06928 [astro-ph.CO] .

O. Akarsu, E. Ó Colgáin, A. A. Sen, and M. M. Sheikh-Jabbari, *Monthly Notices of the Royal Astronomical Society: Letters* **542**, L36 (2025), arXiv:2410.23134 [astro-ph.CO] .

E. P. Longley *et al.* (LSST Dark Energy Science), *Mon. Not. Roy. Astron. Soc.* **520**, 5016 (2023), arXiv:2208.07179 [astro-ph.CO] .

M. Maus *et al.* (DESI), *JCAP* **2025**, 077 (2025), arXiv:2505.20656 [astro-ph.CO] .

R. Stiskalek, “ s_8 from tully-fisher, fundamental plane, and supernova distances agree with planck,” (2025), arXiv:2509.20235 [astro-ph.CO] .

J. U. Lange, A. P. Hearin, A. Leauthaud, F. C. van den Bosch, E. Xhakaj, H. Guo, R. H. Wechsler, and J. DeRose, *Mon. Not. Roy. Astron. Soc.* **520**, 5373 (2023), arXiv:2301.08692 [astro-ph.CO] .

N. Palanque-Delabrouille *et al.*, *JCAP* **04**, 038 (2020), arXiv:1911.09073 [astro-ph.CO] .

M. Abdul Karim *et al.* (DESI), *Phys. Rev. D* **112**, 083515 (2025), arXiv:2503.14738 [astro-ph.CO] .

DESI Collaboration, A. G. Adame, J. Aguilar, S. Ahlen, S. Alam, *et al.*, *Journal of Cosmology and Astroparticle Physics* **2025**, 012 (2025), arXiv:2404.03000 [astro-ph.CO] .

Euclid Collaboration, R. Scaramella, *et al.*, *Astronomy & Astrophysics* **662**, A112 (2022), arXiv:2108.01201 [astro-ph.CO] .